Application of Moire Photography to the Study of Dynamic Fracture

J. M. HUNTLEY and J. E. FIELD
University of Cambridge, Cavendish Laboratory, Madingley Road, Cambridge CB3 0HE, UK

ABSTRACT

The use of moiré photography as a technique for measuring the dynamic displacement field, and dynamic stress intensity factor(K_{Id}) of a fast crack has been investigated. Sequences of double exposure moiré photographs of cracks moving through plates of polymethylmethacrylate (PMMA) were recorded with a rotating mirror camera at 2 μs frame^{-1}. One sequence was analysed in detail to reveal the time variation of both in-plane displacement components, and K_{Id}. The paper ends with a description of a high resolution moiré apparatus, capable of resolving 150 lines mm^{-1}; preliminary results from quasi-statically loaded cracks are presented.

KEYWORDS

Dynamic fracture; dynamic stress intensity factor; moiré photography; automatic fringe analysis.

INTRODUCTION

The measurement of the dynamic stress intensity factor (K_{Id}) at the tip of a fast crack has been the subject of considerable research activity over recent years. Optical techniques which have been applied to the study of dynamic fracture include the method of caustics (Manogg, 1964; Theocaris and Gdoutos, 1972), photoelasticity (Dally, 1979), white light speckle photography (Hu *et al.*, 1984; Peters *et al.*, 1985), holographic interferometry (Rossmanith, 1983), and SIFT (Stress Intensity Factor Tracer) (Kim, 1985). The method of caustics and photoelasticity have become established as the two main techniques for measuring K_{Id}. However, a transparent material exhibiting stress-induced birefringence is required for photoelastic work, and the method of caustics provides only limited information on the stress state near the crack tip. Furthermore, photoelasticity and the method of caustics do not always produce consistent results (Dally, private communication). There is a clear need for improved experimental techniques, in order to resolve important questions such as the uniqueness of the relationship between crack velocity and K_{Id}, and mechanisms for crack branching. For these reasons the technique of moiré photography has been investigated as an alternative method for determining K_{Id}.

DYNAMIC MOIRE PHOTOGRAPHY

In experimental mechanics, the moiré technique refers to the superimposition of two line gratings: one attached to the specimen (specimen grating), the other stationary (reference grating). A fringe pattern is formed which is essentially a contour map of the in-plane displacement component normal to the grating lines, with a contour interval equal to the specimen grating pitch. When both

in-plane components are required, a crossed specimen grating is used; the two fringe patterns representing displacement along the x and y axes are called the u_x- and u_y-field patterns, respectively. Further details of the standard moiré technique are described by Sciammarella (1982).

The application of moiré to dynamic events is not straightforward, however. Firstly, there is insufficient time to rotate the line reference grating through the 90° needed to separate the u_x- and u_y-field patterns. This problem can be overcome by recording images of the specimen grating with a high speed camera; the patterns are then separated by optical spatial filtering (Sciammarella, 1982). The drawback now is that the camera must be able to resolve the grating. High speed cameras have poor spatial resolution, ranging typically from 10–30 lines mm^{-1} (l mm^{-1}) in the image plane. If a specimen grating with a higher spatial frequency is required, the image must be magnified, resulting in a basic trade-off between displacement accuracy (determined by the specimen grating pitch), and field of view. One final point is that the exposure time must be much less than the specimen grating pitch divided by maximum specimen velocity, otherwise the image of the grating will be blurred. In this section, results are presented from a series of high speed photographic sequences of fast crack growth in polymethylmethacrylate (PMMA). In the next section, it is shown how the trade-off between grating pitch and field of view can be eliminated by forming the moiré fringe patterns outside the camera.

For the experiments described in this section, a Beckman and Whitley model 189 rotating mirror camera was used on account of its good spatial and temporal resolution. The specimen grating frequency was 40 l mm^{-1}; although the claimed resolution of the camera is over 30 l mm^{-1}, in practice it was necessary to magnify by about 2.5 times, resulting in an image plane frequency of about 16 l mm^{-1}, and a field of view of 10 × 6 mm^2. The specimen grating was a commercially available stripping film, attached to the specimens by cyanoacrylate adhesive. The specimens were made from cast PMMA (ICI 'Perspex') to dimensions of 40 × 32 × 3 mm^3 (see Fig. 1(a)). A notch was machined on one edge to accept a 'V'-shaped chisel containing a small detonator (ICI fast acting fuze); firing the detonator initiated the crack reproducibly on a microsecond timescale.

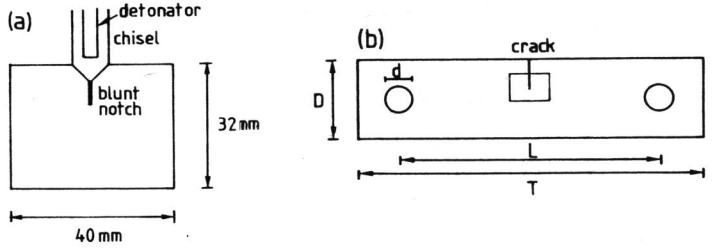

Fig. 1. Specimen geometries for (a) dynamic and (b) quasi-static experiments. Specimen dimensions shown in 1(b): T = 305 mm; L = 229 mm; D = 76 mm; d = 25.4 mm.

A total of seven double exposure sequences were recorded by transmitted light. The film used was Kodak Technical Pan 2415 (nominal speed 50 ASA), developed in Ilford ID11. For each sequence, the first exposures were made by running the camera up to speed and firing the flash. The specimen was then loaded to about half the failure stress, and the magnification was changed by about 2% to produce sufficient mismatch fringes in the final moiré photographs. The second run of the camera fired the detonator and recorded the deforming grid associated with the propagating crack.

Figure 2(a) shows one such doubly exposed frame from one of the sequences, recorded at 2 μs $frame^{-1}$. Subsequent spatial filtering reveals the u_x- and u_y-field fringes at high contrast (Figs. 2(b) and (c)). The u_x pattern is superior because the camera construction results in better spatial resolution for vertical lines than for horizontal lines. The slightly speckled appearance of the

fringes is a result of scattering by the film. Normally when spatially filtering, a much finer grained film would be used; such a film would have been too slow for this application, however. The patterns were analysed manually, by converting the fringe orders to displacement components on a square mesh of 20 × 37 datapoints. The linear displacement field due to the magnification change was then subtracted to give the experimentally observed displacement field resulting from the crack alone, (u_x^{obs},u_y^{obs}).

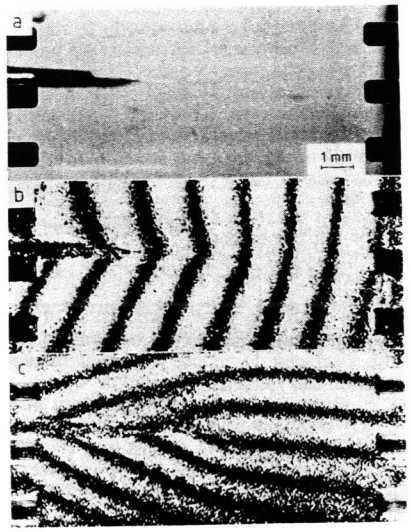

Fig. 2(a). Single frame from sequence of double exposure moiré photographs of fast crack in PMMA, recorded at 2 μs $frame^{-1}$. (b) and (c) are the spatially filtered images of 2(a), revealing the u_x- and u_y-field fringes, respectively.

Least-squares analysis

The dynamic stress intensity factor, K_{Id}, was estimated by minimising the sum

$$S^2 = \sum_{i=1}^{N} \left((u_x^{calc} - u_x^{obs})^2 + (u_y^{calc} - u_y^{obs})^2 \right) \qquad (1)$$

over N datapoints. The superscript *calc* refers to the theoretical dynamic displacement field. In a coordinate system (x,y) moving such that the origin is always at the crack tip, and with the crack lying along the –x axis, the mode I displacements can be expressed as a sum of terms of the form (Nishioka and Atluri, 1983):

$$u_{xn} = \left[K_n{}^{o}B(\dot{a})(n+1)/(2\pi)^{1/2}\mu \right] \left[r_1^{n/2}\cos(n\theta_1/2) - h(n) r_2^{n/2}\cos(n\theta_2/2) \right]$$
$$u_{yn} = \left[K_n{}^{o}B(\dot{a})(n+1)/(2\pi)^{1/2}\mu \right] \left[-s_1 r_1^{n/2}\sin(n\theta_1/2) + (h(n)/s_2) r_2^{n/2}\sin(n\theta_2/2) \right] \qquad (2)$$

where

$$s_1^2 = 1 - \dot{a}^2/c_1^2 \qquad s_2^2 = 1 - \dot{a}^2/c_s^2$$

$$r_1^2 = x^2 + s_1^2 y^2 \qquad r_2^2 = x^2 + s_2^2 y^2$$

$$\tan\theta_1 = s_1 y/x \qquad \tan\theta_2 = s_2 y/x$$

$$c_1^2 = (\kappa+1)\mu/(\kappa-1)\rho \qquad c_s^2 = \mu/\rho$$

$$B(\dot{a}) = (1+s_2^2)/(4s_1s_2-(1+s_2^2)^2)$$

$$h(n) = 2s_1s_2/(1+s_2^2) \quad \text{(n odd)}$$

$$= (1+s_2^2)/2 \quad \text{(n even)}$$

$$\kappa = (3 - \nu)/(1 + \nu) \quad \text{(plane stress)}$$

$$= (3 - 4\nu) \quad \text{(plane strain)} \qquad (3)$$

$\dot{a}$ is the crack speed, ρ the density, μ the shear modulus, and ν Poisson's ratio. The parameters K_n^o represent the contribution of the nth eigenfunction (n = 0,1,2,3...) to the stress field; the singular term corresponds to n = 1, and K_{Id} is K_1^o.

Datapoints within 1.5 mm (half the plate thickness) of the crack tip were excluded from the analysis because of 3-dimensional effects (Yang and Freund, 1985), and points more than 2.5 mm from the tip were also excluded to reduce boundary influences. Plane stress conditions were assumed to prevail within this annulus of eligible datapoints. In the analysis, the first two parameters K_1^o and K_2^o, together with the two rigid body in-plane displacement components (Δx and Δy) and rotation (Ω) were allowed to vary. The average crack velocity was measured as 380 ± 30 m s^{-1} from a plot of crack length against time (Fig. 3(a)). The loading time for a point a distance r from the crack tip is $\tau \approx r/\dot{a}$ around 10^{-5} s in these experiments. The appropriate values for Young's modulus, E, and Poisson's ratio, ν, on this timescale are 5.65 GPa and 0.34, respectively (Read and Dean, private communication).

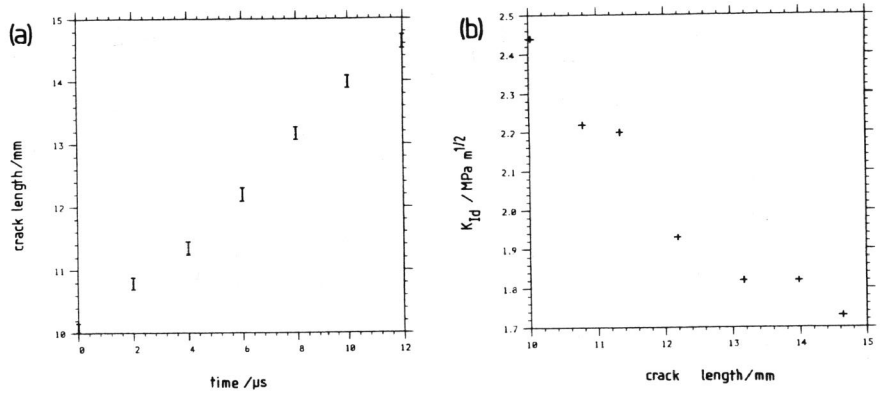

Fig. 3. (a) Crack length as a function of time. The total length of the blunt starter notch (including the 'V' notch) was 10.0 mm. (b) K_{Id} as a function of crack length, as calculated by a linear least squares method from the moiré fringe patterns.

Seven frames were analysed in this way, and the results are plotted in Fig. 3(b). K_{Id} appears to have fallen from an initial value of over 2.4 MPa $m^{1/2}$ (frame 1) to just over 1.7 MPa $m^{1/2}$ (frame 7). The K_{Id} values are subject to systematic errors, resulting mainly from the magnification change between exposures, which may be as high as 15%. Nevertheless, the drop in K_{Id} is significant. A plausible explanation for the behaviour is as follows. The apparently high initial toughness of the material is due to initiation from a blunt starter notch, rather than from a sharp crack. Once the crack starts to move, release waves from the crack tip act to reduce the stress intensity factor, but dynamic effects prevent this from happening instantaneously. Theoretical and numerical work by Freund (1973) and Sih (1973) showed that a step function stress pulse incident on a crack causes K_{Id} to change with time, t, initially as $t^{1/2}$, before reaching the steady-state value after a time roughly equal to the time taken by a longitudinal wave to travel twice the length of the crack. Based on the initial notch length of 10 mm, and a longitudinal wave speed of 2300 m s^{-1}, the expected response time is about 10 μs for the experiments described here. Although no record exists for K_{Id} after frame 7, fracture surface markings showed that the crack did not arrest, suggesting a lower bound of 1.6 MPa $m^{1/2}$, the K_{Ic} value for Perspex (Williams, 1984). It is clear then from Fig. 3 that the significant drop in K_{Id} does indeed occur over a timescale of about 10 μs. It is generally accepted that the fracture toughness of brittle polymers increases with crack velocity; the changes in K_{Id} described above, however, occur without obvious correlation with the crack speed (given by the gradient of Fig. 3(a)). More detailed studies on the uniqueness of the relationship between fracture toughness and crack velocity will be carried out using the technique described in the next section.

HIGH RESOLUTION MOIRE PHOTOGRAPHY

In this section, an alternative technique for simultaneously visualising both in-plane displacement components is described, and preliminary results are presented from experiments to measure the quasi-static displacement field around a crack tip.

The experimental arrangement is shown in Fig. 4. The basic principle is that a crossed specimen grating is imaged onto a crossed reference grating. A set of crossed linear mismatch fringes (or "carrier" fringes) is produced by choosing a magnification of slightly greater than unity. The fringes will distort as the specimen deforms, but provided the mismatch fringes have a sufficiently high spatial frequency, the u_x- and u_y-field fringes do not become parallel at any point in the field of view, and can therefore be subsequently separated. The required frequency of the carrier fringes will, however, be generally much less than the spatial frequency of the specimen grating, so that the fringes can be recorded even by a camera with only limited spatial resolution.

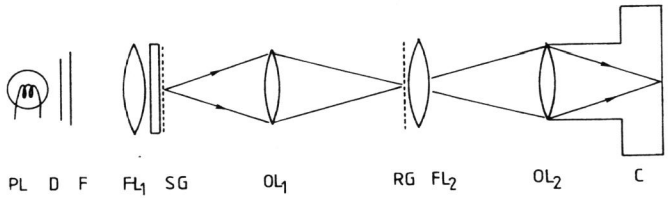

Fig. 4. Experimental arrangement for high resolution moiré photography. PL: projector lamp; D: ground glass diffuser; F: filter (Kodak Wratten No. 44); FL_1, FL_2: field lenses; SG: specimen grating; RG: reference grating; OL_1: high quality objective lens with masked aperture; OL_2,C: recording camera with lens.

Formation of the fringes outside the camera in this way considerably relaxes the basic trade-off between the spatial frequency of the specimen grating and the field of view mentioned earlier. For the experiments described here, the specimen grating frequency was increased to 150 l mm^{-1} (cf. 40 l mm^{-1}), and the field of view was enlarged to 26 × 36 mm^2 (cf. 6 × 10 mm^2). A high quality objective lens (OL_1) is required to resolve 150 l mm^{-1} at a magnification of unity. An Olympus 35 mm SLR camera lens was found to be satisfactory (focal length 80 mm, f/4 macro). The lens was tuned to the spatial frequency of the specimen grating by masking the iris (Burch and Forno,

1982). This reduced the effect of lens aberrations, and increased the fringe contrast. Field lens FL_2 images the iris plane of OL_1 onto the iris plane of objective lens OL_2. The fringe contrast can be improved still further by replacing the reference grating with one of half the specimen spatial frequency (75 l mm^{-1}), and stopping OL_2 down so that it collects only the diffracted beams inside the image of the mask. The interpretation of the moiré fringe pattern remains unchanged; the theory behind this modification will be published elsewhere.

Single edge notch (SEN) specimens of PMMA (dimensions 305 × 76 × 6 mm^3) were used for the experiments described here. The specimen geometry is shown in Fig. 1(b). Both reference and specimen gratings were created on holographic emulsion Agfa 10E75 by two-beam interference from a He-Ne laser: the former on a glass plate; the latter on polyester film. Conventional stripping film was not sufficiently fine-grained. The drawback of the polyester is that although only 100 μm thick, it inhibits crack growth in the PMMA due to its high fracture toughness. After the gratings were attached with cyanoacrylate adhesive, a groove 0.35 mm wide was therefore machined through the polyster, down to the PMMA substrate, along the expected path of the crack. In each specimen, a sharp crack was initiated from the blunt starter notch with a razor blade, and grown to the required length by loading the specimen at $K_I \approx 0.9$ MPa m$^{1/2}$. A moiré fringe pattern from one of the specimens is shown in Fig. 5.

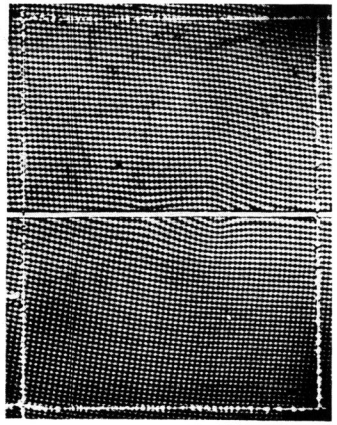

Fig. 5. Moiré fringe pattern around a quasi-statically loaded crack in PMMA. The position of the scribed rectangle (dimensions 26 × 36 mm^2) on the specimen is shown in Fig. 1(b); the crack is in the conventional orientation, with the tip at the centre of the rectangle. The specimen grating frequency is 150 l mm^{-1}.

Computer analysis of fringe patterns

One drawback to the technique described in the previous section was the time taken to convert the information in the fringe patterns to displacement data suitable for least-squares analysis. Analysis of the seven frames, which covered an event lasting 12 μs, took approximately 50 man hours. It will be shown here how crossed carrier fringe patterns (such as Fig. 5) can be analysed automatically by computer.

The image processing technique is based on the Takeda Fourier transform method (Takeda *et al.*, 1982). The original technique was applied to one set of fringes, but it also works well with two sets of crossed fringes, provided the carrier frequencies of the two fringe patterns are sufficiently high. 2-D Fourier transformation of the fringes reveals five peaks: two for the u_x fringes; two for

the u_y; and one representing the d.c. term. One of the fringe peaks is isolated, with the remainder of the transform plane being set to zero; this is then followed by an inverse Fourier transform. The image is now a complex 2-D array, where the phase at any point equals the phase of the corresponding fringes, but wrapped onto the range 0 to 2π. For example, selection of the positive u_x peak results in a phase map which will be denoted by $\Phi_x(x,y)$. Repeating the process with a fringe pattern recorded after loading the specimen results in a second phase map. The difference between the post-load and pre-load maps, $\Delta\Phi_x$, is shown in Fig. 6(a). The equivalent map, $\Delta\Phi_y$, representing the u_y displacement component, is shown in Fig. 6(b). The computer unwraps the phase maps automatically, starting at the top right hand corner and working down each column, looking for absolute jumps in phase of greater than π. Depending on the sign of the jump, 2π is either added to or subtracted from the remaining elements of the column. The process is repeated, starting again at the top right hand corner, but now working along the rows. Once the two difference phase maps have been unwrapped, the displacement components are calculated as

$$u_x = p_s\Delta\Phi_x/2\pi$$
$$u_y = p_s\Delta\Phi_y/2\pi \qquad (4)$$

where p_s is the pitch of the specimen grating (6.58 μm). The slight asymmetry of the phase maps about the crack line is due to the grating not lying precisely along the x-y coordinate system of the crack. In this case the misalignment was 5.46°. Once the vector displacement field has been calculated by eqn. (4), a simple rotation matrix is therefore applied to give the true u_x and u_y components.

The value of K_I was estimated by least-squares analysis, as in the previous section. In this case, the crack was stationary so the quasi-static form of eqn. (2) could be used. Based on the timescale of 100 s between applying the load and recording the photograph, Young's modulus and Poisson's ratio were taken to be 3.08 GPa and 0.35, respectively. The stress intensity factor resulting from the analysis of the phase maps shown in Fig. 6 was 0.490 MPa m$^{1/2}$, which compares well with the value of 0.501 MPa m$^{1/2}$ calculated from the applied load.

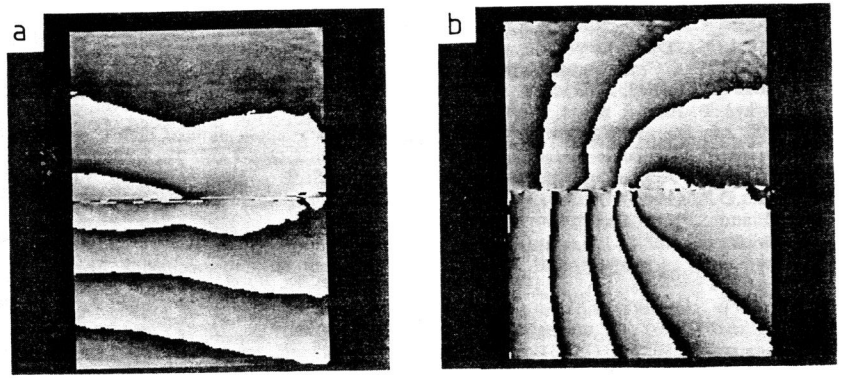

Fig. 6. Difference phase maps $\Delta\Phi_x$ (a) and $\Delta\Phi_y$ (b) showing the u_x and u_y displacement components resulting from mode I loading of the crack. The region covered corresponds to the scribed rectangle in Fig. 5 (dimensions 26 × 36 mm^2). The phase ranges from 0 (black) to 2π(white); the phase discontinuities occur at intervals of 2π, representing a relative displacement equal to the specimen grating pitch, 6.58 μm.

CONCLUSIONS

It has been shown how the techniques of moiré photography and high speed photography can be combined to measure the in-plane displacement field around the tip of a fast crack. Double exposure photographs were recorded with a rotating mirror camera at 2 μs frame^{-1}, and subsequently spatially filtered to generate u_x- and u_y-field fringe patterns. K_{Id} was calculated by least-squares analysis of the displacement field. An improved arrangement was proposed in which the camera records the moiré fringes, rather than the specimen grating. Quasi-static tests were carried out with a specimen grating frequency of 150 l mm^{-1}. The errors in stress intensity factor were estimated to be up to 15% for the dynamic experiments, reducing to 2% for the static tests with the improved apparatus.

Moiré techniques appear to offer important advantages over photoelasticity and the method of caustics. Photoelasticity requires thick specimens to achieve the necessary sensitivity; to avoid the region of triaxial stress, datapoints well away from the crack tip are therefore used to calculate K_{Id}, and this may introduce appreciable errors when K_{Id} is changing rapidly. In the dynamic experiments described here, all the datapoints were within 2.5 mm of the crack tip. The method of caustics relies on out-of-plane displacements, which are thought to respond more slowly than in-plane displacements to a changing in-plane stress field. The main disadvantage of the moiré method, the data processing time, is significantly reduced by the automatic fringe analysis technique described in this paper.

ACKNOWLEDGMENTS

We are grateful to N. Wilson and M. F. Turner for initial experimental work. One of us (J.M.H.) was supported by Research Fellowships from Gonville and Caius College, Cambridge and from the Science and Engineering Research Council.

REFERENCES

Burch J. M. and C. Forno (1982). High resolution moiré photography, *Opt. Eng.*, 21, 602-614.

Dally, J. W. (1979). Dynamic photoelastic studies of fracture. *Exp. Mech.*, 19, 349-361.

Freund L. B. (1973). Crack propagation in an elastic solid subjected to general loading-III. Stress wave loading. *J. Mech. Phys. Solids*, 21, 47-61.

Hu X. M., S. J. P. Palmer and J. E. Field (1984). The application of high speed photography and white light speckle to the study of dynamic fracture. *Opt. Laser Tech.*, 303-306.

Kim K.-S. (1985). A stress intensity factor tracer, ASME *J. Appl. Mech.*, 52, 291-297.

Manogg P. (1964). Anwendung der Schattenoptik zur Untersuchung des Zerreissvorganges von Platten. Ph.D. Thesis, University of Freiburg.

Nishioka T. and S. N. Atluri (1983). Path-independent integrals, energy release rates, and general solutions of near-tip fields in mixed-mode dynamic fracture mechanics. *Eng. Fract. Mech.*, 18, 1-22.

Peters W. H., W. F. Ranson, J. F. Kalthoff and S. R. Winkler (1985). A study of dynamic near-crack-tip fracture parameters by digital image analysis. *J. de Physique*, 46, C5–631-638.

Rossmanith, H. P. (1983). Determination of dynamic stress-intensity factors by holographic interferometry, *Opt. Lasers Eng.*, 4, 129-143.

Sciammarella C.A. (1982). The moiré method- a review, *Exp. Mech.*, 22, 418-433.

Sih G. C. (1973) Handbook of stress intensity factors, Lehigh University.

Takeda M., H. Ina and S. Kobayashi (1982). Fourier transform method of fringe-pattern analysis for computer-based topography and interferometry, *J. Opt. Soc. Am.*, 72, 156-160.

Theocaris P. S. and E. E. Gdoutos (1972). An optical method for determining opening-mode and edge sliding-mode stress intensity factors. ASME *J. Appl. Mech.*, 39, 91-97.

Williams J. G. (1984). *Fracture mechanics of polymers*. John Wiley and Sons.

Yang W. and L.B. Freund (1985). Transverse shear effects for through-cracks in an elastic plate. *Int. J. Solids Struct.*, 21, 977-994.